Double cores of the Ozone Low in the vertical direction over the Asian continent in satellite data sets

Zhou Tang[1], Dong Guo[1,4]*, YuCheng Su[1,5], ChunHua Shi[1,4]*, ChenXi Zhang[1], Yu Liu[2], XiangDong Zheng[2], WenWen Xu[1], JianJun Xu[3,4], RenQiang Liu[1], and WeiLiang Li[2]

[1]Key Laboratory of Meteorological Disaster, Ministry of Education/Joint International Research Laboratory of Climate and Environment Change/Collaborative Innovation Center on Forecast and Evaluation of Meteorological Disasters, Nanjing University of Information Science & Technology, Nanjing, 210044 China;

[2]Chinese Academy of Meteorological Sciences, Beijing, 100081 China;

[3]Guangdong Ocean University, Zhanjiang, 524088 China;

[4]The Global Environment and Natural Resources Institute (GENRI), College of Science, George Mason University, Fairfax, 22030 USA;

[5]Center for Atmospheric Science, Hampton University, Hampton, 23668 USA

Abstract: Using four satellite data sets (TOMS/SBUV, OMI, MLS, and HALOE), we analyze the seasonal variations of the total column ozone (TCO) and its zonal deviation (TCO*), and reveal the vertical structure of the Ozone Low (OV) over the Asian continent. Our principal findings are: (1) The TCO over the Asian continent reaches its maximum in the spring and its minimum in the autumn. The Ozone Low exists from May to September. (2) The Ozone Low has two negative cores, located in the lower and the upper stratosphere. The lower core is near 30 hPa in the winter and 70 hPa in the other seasons. The upper core varies from 10 hPa to 1 hPa among the four seasons. (3) The position of the Ozone Low in the lower and the upper stratosphere over the Asian continent shows seasonal variability.

Keywords: Ozone Low; Double core; Asian continent; Satellite data

1. Introduction

The ozone layer is important not only to stratospheric and tropospheric climate (Andrews et al., 1987; Xie F et al., 2016; Zhang JK et al., 2018; Guo D et al., 2017a), but also to ecological systems (Fuhrer and Booker, 2003). Without the ozone layer, humans, animals, and plants could not live (Van der Leun et al., 1995). Molina and Rowland (Molina and Rowland, 1974) discovered that chlorofluorocarbons were thinning the ozone layer. Furthermore, great ozone loss was found over the South Pole (Farman et al., 1985) and in the Arctic (Newman et al., 1997). Therefore, ozone depletion attracted much attention. Meanwhile, a similar pattern of ozone depletion was found in the middle latitudes. Based on Total Ozone Mapping Spectrometer (TOMS) data, Zhou XJ et al. (1994) first found a noticeable low value center by comparing the TCO over the Tibetan Plateau (TP) with the eastern part of China at the same latitude. Zou H (1996), however, calculated the zonal deviations of global total ozone in different seasons of 1979–1991 using TOMS data, confirming the Ozone Low by zonal deviations. But these definitions of the Ozone Low are not the same and do

not have a quantitative indicator. Bian JC et al. (2006) reported an unusual Ozone Low in the winter over the TP based on longer TOMS datasets. Recently, Guo D et al. (2015) found a double core structure of the Ozone Low using the Aura Microwave Limb Sounder (MLS) data. Besides analyses of the phenomenon, there are some studies on the Ozone Low mechanism (Guo D et al., 2017a, b ; Li ZK et al., 2017). In previous studies, the contribution of the dynamic process to the formation of the OV was associated with the South Asian High (SAH) (Liu Y et al., 2003; Li ZK et al., 2017; Tian WS et al., 2008; Qin H et al., 2018; Guo D et al., 2012). Moreover, many studies have suggested that dynamic effects dominate the Ozone Low formation while stressing that the chemical effect is also a possible factor. Fu C et al. (1997), Liu Y et al. (2010), and Guo D et al. (2015) emphasize the chemical factors. Tian WS et al. (2008) claimed that the atmospheric column loss, which is impacted by the terrain, can partly explain the results in column ozone loss. There are also other studies focused on detailed features of the Ozone Low (Ye ZJ and Xu YF, 2003; Zhou SW and Zhang RH, 2005; Moore and Semple, 2005; Tobo et al., 2008; Liu Y et al., 2009; Zhang JK et al., 2014). In addition, the Ozone Low is found not only over the TP, but also over the Iranian Plateau (IP) (Wang WG et al., 2006; Yan RC et al., 2011).

However, those studies on the Ozone Low do not have a unified criterion and show varying uncertainties in the different datasets. Furthermore, previous studies do not consider the seasonal

change of the Ozone Low. To clarify these problems, we examine similarities and differences of the Ozone Low using four satellite observation and one observation datasets (described in the following section). Section 3 presents seasonal variation and vertical structure of the Ozone Low. Sections 4 and 5 present discussion and conclusions.

2. Materials and Methods

2.1 Data

We considered four satellite observations and one observation data. They are briefly described below.

The Total Ozone Mapping Spectrometer and the Solar Backscattered Ultraviolet merged data version 8 (TOMS/SBUV) includes measurements from six satellites: Nimbus 7 TOMS, Nimbus 7 SBUV, NOAA 9, 11, and 16 SBUV/2s, and Earth Probe TOMS. The TOMS and SBUV instruments measure the total column ozone (TCO) by mapping backscattered ultraviolet radiation (Heath et al., 1975; Frederick et al., 1986; Hilsenrath et al., 1995; McPeters and Labow, 1996; McPeters et al., 1998). In this paper, TOMS data are used for total column ozone (TCO). The resolution of the TCO is 1° × 1.25° (latitude × longitude) and temporal coverage is from November 1980 to December 1992.

The Ozone Monitoring Instrument data version 3 (OMI) was launched on NASA's Earth Observing System's Aura satellite. OMI measures backscattered hyperspectral radiation in the range of 270–500 nm in three channels (Levelt et al., 2006). We use OMI data for total column ozone (TCO). The resolution of the TCO is 1° × 1° (latitude × longitude) and temporal coverage is from January 2005 to December 2014.

The Microwave Limb Sounder on the Aura satellite data v4.2 (MLS) instrument was launched on the Aura satellite. It looks through the atmospheric limb along the orbital track and obtains a vertical ozone (O_3) profile by scanning the field of view up and down (Waters et al., 1999, 2004, 2006). Because MLS detects microwave emissions, this instrument measures ozone profiles during both the daytime (ascending) and nighttime (descending). Moreover, the number of observations in the day and night times are almost the same. Much rigorous and detailed verification work has been done to evaluate the MLS data (Yan XL et al., 2015; Shi CH et al., 2017). We use MLS satellite data v4.2 (MLS) both for the total column ozone and for the vertical profiles of ozone (O_3). The resolution of the TCO is 1° × 1° (latitude × longitude) and temporal coverage is from January 2005 to December 2014 for the total column ozone. The total column ozone in MLS represents the ozone concentration in the stratosphere. But for the vertical profiles of ozone, the horizontal resolution of the ozone is 2° × 2° and temporal coverage is from January 2005 to December 2014. There are 55 layers of the ozone in the vertical direction. In addition, the ozone unit is parts per million by volume (ppmv). More publications on MLS can be obtained from the website of the Jet Propulsion Laboratory.

The Halogen Occultation Experiment data version 19 (HALOE) was launched on the Upper Atmosphere Research Satellite (Russell III et al., 1993, 1994). The experiment uses solar occultation to measure vertical profiles of ozone (O_3) and other tracers. HALOE tracks the top edge of the Sun. There are no systematic differences in the tracking procedures and no significant biases in the record between sunrise and sunset (Nazaryan et al., 2005). The horizontal resolution of the ozone in this article is 5° × 5° and temporal coverage is from January 1992 to December 2005. There are 271 layers of the ozone in the vertical direction.

2.2 Methods

If the variable is F, its zonal deviation is F^*. The F^* can be expressed as $F^* = F - [F]$. Here [F] is zonal mean of F. According to this definition, the zonal deviation (TCO^*) of the total column ozone (TCO) and the zonal deviation (O_3^*) of the ozone concentration profile (O_3) will be investigated. The smaller the negative values of TCO^* and O_3^*, the stronger the Ozone Low. In this work, the TP area is defined as 25°N to 40°N, 80°E to 100°E. The integrated column Z (units: DU) can be calculated as follows (Bian JC et al., 2011):

$$Z_{p_1}^{p_2} = \int_{p_1}^{p_2} 0.789\, M\, \mathrm{d}P,$$

Here, P is the pressure (units: hPa) and M is the mixing ratio of volume (units: ppmv).

3. Results

3.1 Seasonal Variability of the TCO

The TCO on the Asian continent shows seasonal variability in different periods for different datasets (Figure 1). A trough of the TCO can be found over the TP in all four seasons. Over the TP, an Ozone Low is identified in spring (March, April, and May, short as MAM) in the OMI and TOMS satellite observations. The value is about 290 DU in the TOMS and 280 DU in the OMI. Obviously, the Ozone Low becomes lower in the summer (June, July, and August, short as JJA), where a value of 270 DU is both observed in the TOMS and OMI. And the scope of the Ozone Low is enlarged. In the autumn (September, October and November, short as SON), the Ozone Low drops to 255 DU in the OMI and TOMS observations. In the OMI, the scope of the Ozone Low is reduced in winter (December-February, short as DJF). The Ozone Low is about 260 DU over the TP. However, the OV disappears in the TOMS data. Over the TP, a very weak trough is identified in the winter. The TCO shows a quite different seasonal change in the MLS satellite observations; the Ozone Low appears only in the summer. There exists a closed center controlling the western side of the Asian continent. Additionally, we can find a low trough in Spring and Autumn on the Asian continent.

It is obvious that the TCO shows a seasonal variation over the TP area. To display clearly the seasonal changes in intensity of the Ozone Low, the multi-year-average of the TCO over the TP has been calculated. Figure 2 shows that the lowest value of the TCO occurs in October and the highest in April in the TOMS data and in March in the OMI data. Thus, we can conclude that the TCO over the TP reaches its maximum in the spring and its minimum in the autumn. Error bars indicate ±2 standard deviations. The standard deviation reaches the maximum in February in the OMI and MLS and in March in the TOMS, which means that there is a great un-
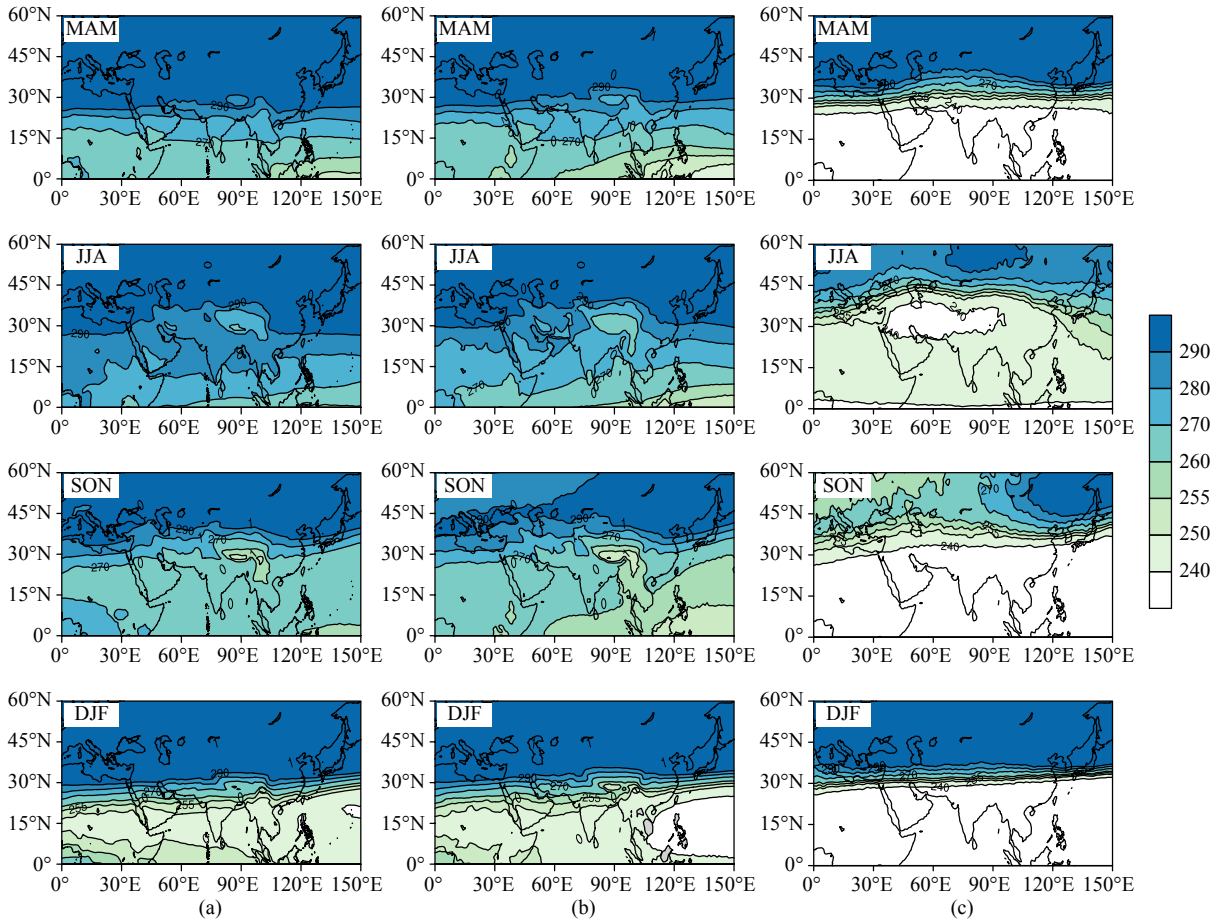
Figure 1. The latitude–longitude cross sections of mean total column ozone (DU) from (a) TOMS/SBUV, (b) OMI and column ozone in stratosphere from (c) MLS in Spring (March, April, May, short as MAM), in Summer (June, July, August, short as JJA), in Autumn (September, October, November, short as SON) and in Winter (December, January, February, short as DJF).
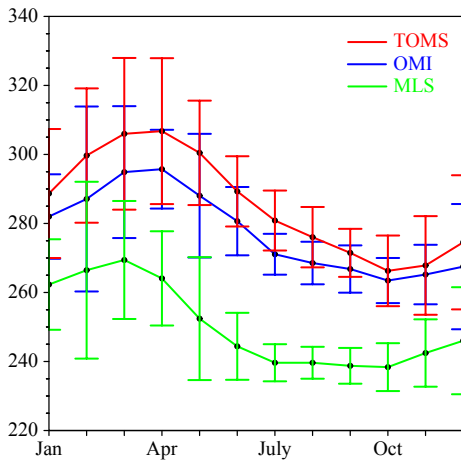
Figure 2. The mean annual cycle of the total column ozone over the TP from TOMS/SBUV (red), OMI (blue) and column ozone in stratosphere from MLS (green). The unit is DU and error bars indicate ±2 standard deviations.

certainty of the TCO in the spring and winter.

3.2 Seasonal Variability of the TCO*

TCO* also shows a seasonal variation of pattern and intensity in different datasets (Figure 3). In the spring, there exists a negative value center about −25 DU near the TP in the TOMS and OMI. A negative value center about −20 DU can be found on the northwest of the TP in the MLS. There exist two negative value centers in the summer in the TOMS and OMI. One is about −25 DU over the TP, the other is about −20 DU over the Iranian Plateaus (IP). In the MLS, two negative value centers can be also found, which are to the north of those in the other datasets. One is over the Caspian Sea with the center value about −25 DU, the other is about −20 DU over the TP. In the autumn, a negative value center about −15 DU can be observed over the TP in the TOMS and OMI. The IP is still dominated by negative TCO*, but the negative value center disappears. The TCO* centers can be identified over the TP in the TOMS and OMI only in winter, with the central value about −10 DU. By contrast, TCO* shows a quite different pattern in the MLS in the autumn and winter. There are no obvious negative value centers on the Asian continent. Furthermore, a positive value center can be detected over the TP in the winter.

The TP area average of the TCO* is shown in Figure 4. Error bars indicate ±2 standard deviations. Compared to the multi-year-average of the TCO (Figure 2), the TCO* shows (Figure 4) totally different results. In the datasets, the TP area average of the TCO* is lowest in May and highest in January. It also reflects that the Ozone Low is strong in summer and weak in winter over the TP accord-
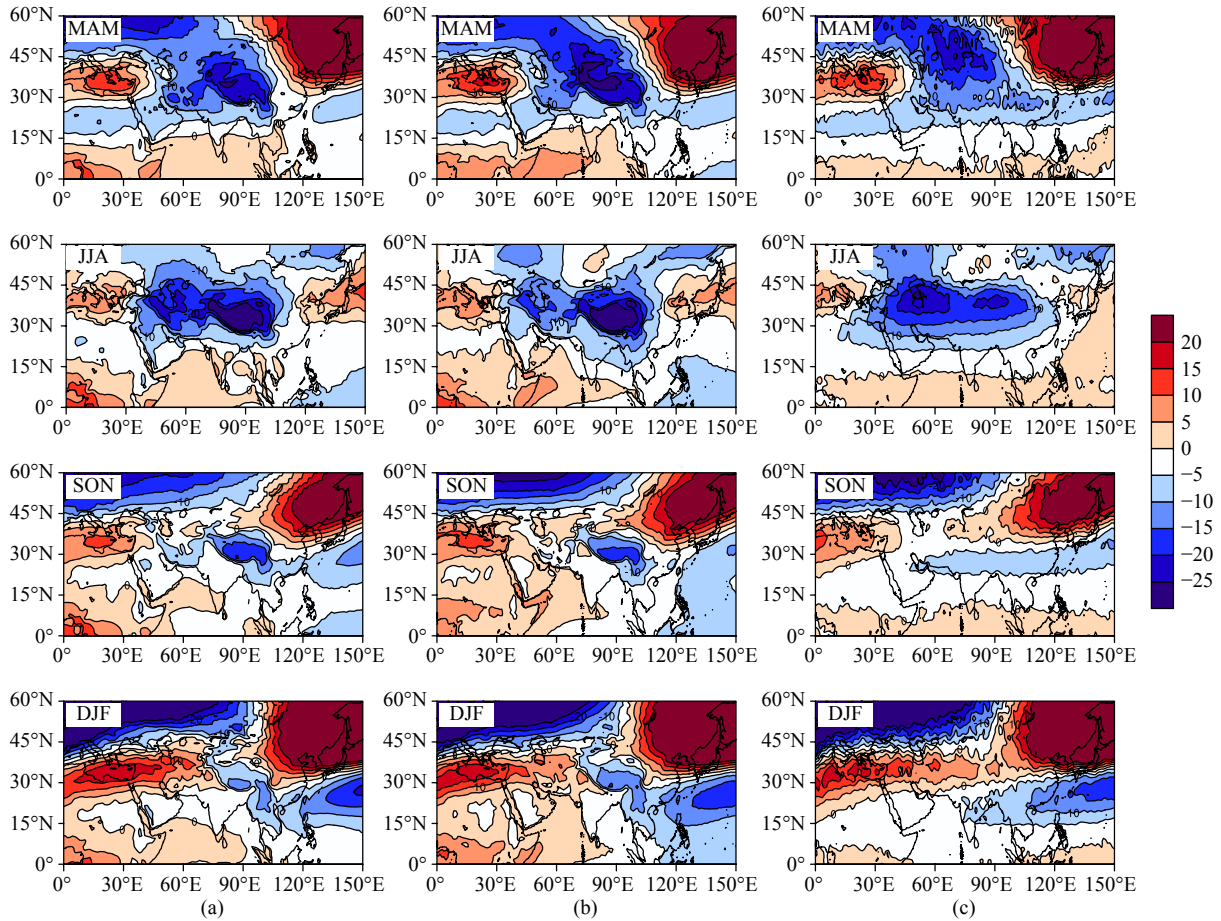
Figure 3. The latitude–longitude cross sections of mean total column ozone zonal deviation (DU) from (a) TOMS/SBUV, (b) OMI and column ozone in stratosphere from (c) MLS in Spring (March, April, May, short as MAM), in Summer (Jun, July, August, short as JJA), in Autumn (September, October, November, short as SON) and in Winter (December, January, February, short as DJF).
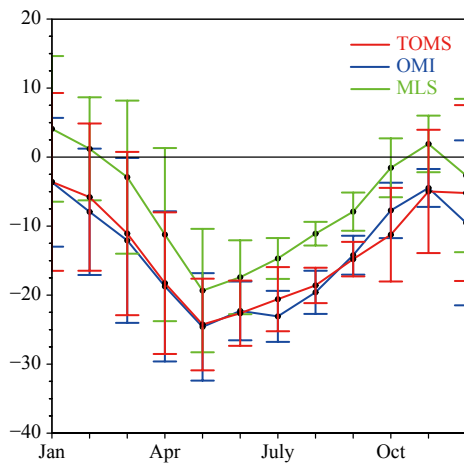
Figure 4. The mean annual cycle of the total column ozone zonal deviation over the TP from TOMS/SBUV (red), OMI (blue) and column ozone in stratosphere from MLS (green). The unit is DU and error bars indicate ±2 standard deviations.

ing to the latitudinal distribution of ozone. If all the data obey the standard normal distribution, when error bars of all data for each data set are under the zero line in a month, there is at least a 95% possibility of the Ozone Low occurrence in that month. Hence, ac-

cording to that condition, we find that the Ozone Low exists from May to September.

In summary, we conclude that the TCO over the TP reaches its maximum in the spring and its minimum in the autumn. The Ozone Low is strong in summer over the TP. There are obvious negative values of the TCO* over the TP from May to September.

3.3 Vertical Structure of the Ozone Low

Over the TP, the ozone maximum concentration in volume relative mixing ratio is in the middle stratosphere in all four seasons (figure omitted). The peak intensity is higher in the spring and summer. But the ozone deviation O_3^* has two negative cores, located in the lower and the upper stratosphere (Figure 5).

The vertical structure of the O_3^* over the TP shows a similar pattern in the MLS and HALOE, and the position and intensity of the O_3^* extremum exhibit seasonal variability. In the lower stratosphere, the extreme value of the O_3^* is close to 30 hPa in the winter but 70 hPa in the spring, summer, and autumn. The extremum is slightly smaller in the spring and summer. The extremum is negative. Thus, the lower core of the Ozone Low is stronger in the spring and summer. Moreover, there exist error bars of the O_3^* in the lower stratosphere less than zero in the summer in all data. Therefore, it is certain that there exists an ozone negative
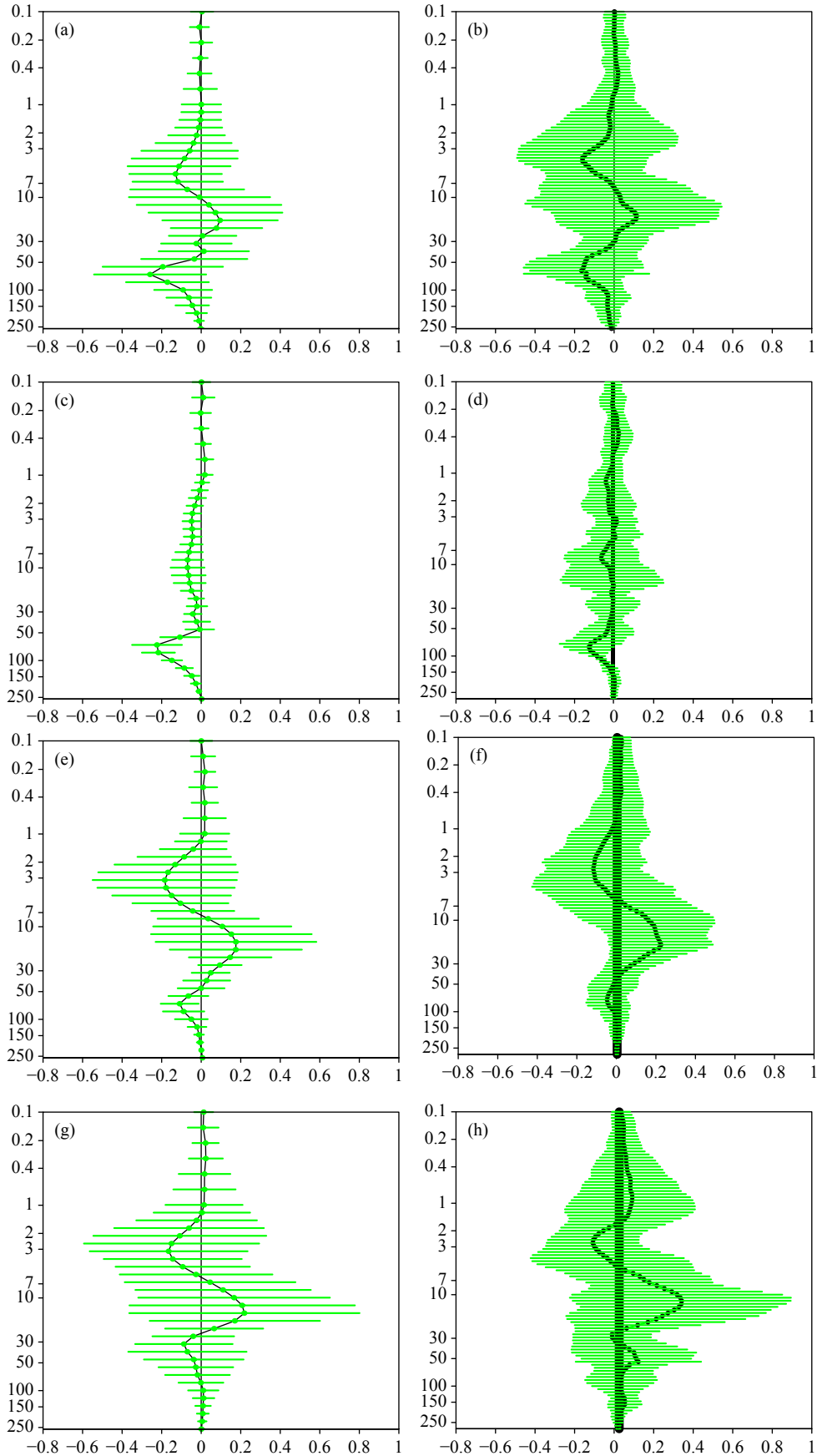
Figure 5. The mean zonal deviation of ozone concentration over the TP in four seasons from MLS (a, c, e, g) and HALOE (b, d, f, h). The unit is ppmv and error bars indicate ±2 standard deviations. (a, b) Spring ; (c, d) Summer; (e, f) Autumn; (g, h) Winter.

Tang Z et al.: Double cores of Ozone Low over Asian continent

value area in the lower stratosphere in the summer.

The positions of the upper cores vary from 10 hPa to 1 hPa in all four seasons in the MLS and HALOE data. The extreme value of the O_3^* is larger in the spring and summer, which is on the contrary to the extremum in the lower stratosphere. Comparing the value of the upper core and the lower core, the extremum in the lower stratosphere is slightly bigger in the spring and summer, while in the autumn and winter, the extremum of the upper layer is slightly bigger.

In order to determine the horizontal pattern of the Ozone Low, we calculated the vertical integration (100–30 hPa and 10–1 hPa) of mean O_3^* in the four seasons.

The vertical integration in the upper stratosphere from 10 hPa to 1 hPa in the MLS and HALOE data (Figure 6) shows that there exists a negative value center about –0.5 DU over the TP in the spring. By summer, the negative value center has shifted slightly to the northwest, with the value center around –0.5 DU in the MLS. However, the negative value center disappears in HALOE. In the autumn, the ozone negative center moves in the two datasets to the eastern part of China at the same latitude with the TP. In the winter, the ozone negative center moves out of the Asian continent. Meanwhile, there are still negative areas over the TP, and the

value of O_3^* can reach –0.5 DU, lower than that in the spring and summer. This can explain why the upper centers of the TP are relatively stronger in the autumn and winter over the TP in Figure 5 although the negative value center of the continent of Asia is not over the TP.

In contrast, the integration from 100 to 30 hPa shows some different characteristics (Figure 7). In the spring, O_3^* negative values occupy the whole Asian area. In the MLS data, the O_3^* negative center is located on the west of the TP. The center value reaches –12 DU. In the HALOE data, the O_3^* negative center is located above the TP, and the center reaches –8 DU. In summer, the O_3^* negative center is over the Caspian Sea, with the center value about –12 DU in the MLS and –8 DU in HALOE. In the autumn, in the MLS there is a large negative center around –4 DU on the west of the TP; in the HALOE, however, the negative center about –4 DU can be observed just over the IP. In the winter, no obvious ozone negative center appears on the Asian continent in either of the two datasets.

4. Discussion

The seasonal variability of the TCO* is quite different from the vertical integration (100–30 hPa and 10–1 hPa) of the mean O_3^* in the
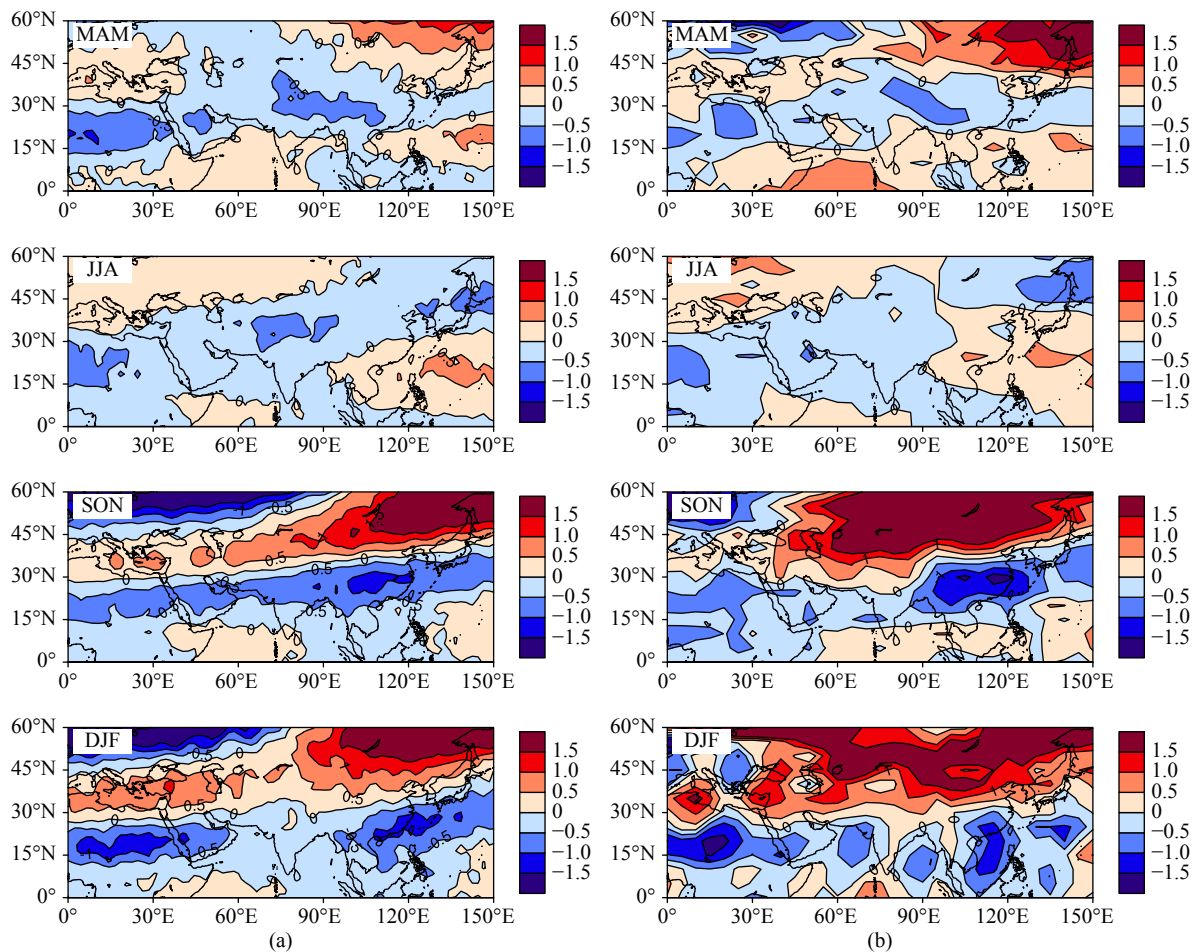
Figure 6. The latitude-longitude cross sections of the vertical integration (10–1 hPa) of mean ozone concentration zonal deviation (DU) in the four seasons, from (a) MLS and (b) HALOE.

Tang Z et al.: Double cores of Ozone Low over Asian continent
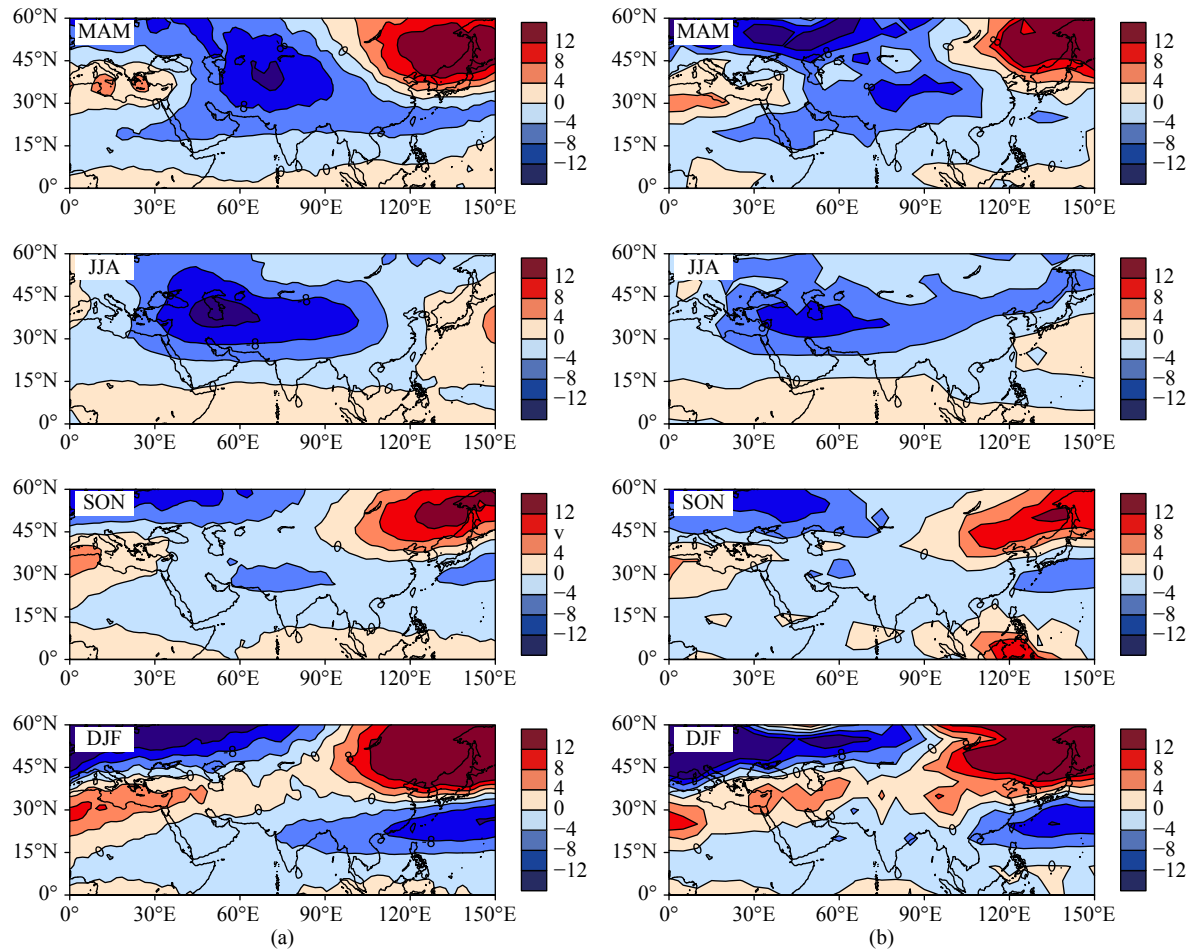
Figure 7. The latitude–longitude cross sections of the vertical integration (100–30 hPa) of mean ozone concentration zonal deviation (unit: DU) in four seasons from (a) MLS and (b) HALOE.

four seasons. The possible reason for this result may be the unique terrain of the TP. In addition, the Ozone Low is found not only over the TP in the lower and the upper stratosphere. The position of the Ozone Low on the Asian continent changes with the seasons, which needs further study.

5. Conclusions

By using four satellite data sets (the TOMS/SBUV, the OMI, the MLS and the HALOE), we have analyzed seasonal variations of the TCO and TCO* and revealed the vertical structure of the Ozone Low.

The results are described below: (1) The TCO over the TP reaches the maximum in the spring and reaches the minimum in the autumn. The Ozone Low exists from May to September. (2) The ozone deviation O_3^* over the TP has two negative cores, located in the lower and in the upper stratosphere. The lower core is near 30 hPa in the winter and 70hPa in the other seasons. The upper core varies from 10 to 1 hPa among the four seasons. The lower core of the Ozone Low in the lower stratosphere is stronger in the spring and summer. The opposite is true in the upper layer. (3) According to the ozone content of the upper stratosphere, the Ozone Low on the Asian continent exists except in the winter in MLS and in the spring and autumn in HALOE. But for the lower stratosphere, the Ozone Low on the Asian continent exists in all sea-

sons except the winter. The position of the Ozone Low in the lower and the upper stratosphere on the Asian continent shows seasonal variability.

References

Andrews, D. G., Holton, J. R., and Leovy, C. B. (1987). *Middle Atmosphere Dynamics* (pp. 12). New York: Academic Press.

Bian, J. C., Wang, G. C., Chen, H. B., Qi, D. L., Lü, D. R., and Zhou, X. J. (2006). Ozone mini-hole occurring over the Tibetan Plateau in December 2003. *Chin. Sci. Bull.*, *51*(7), 885–888. https://doi.org/10.1007/s11434-006-0885-y

Bian, J. C., Yan, R. C., Chen, H. B., Lü, D. R., and Massie, S. T. (2011). Formation of the summertime ozone valley over the Tibetan Plateau: The Asian summer monsoon and air column variations. *Adv. Atmos. Sci.*, *28*(6), 1318–1325. https://doi.org/10.1007/s00376–011-0174–9

Farman, J. C., Gardiner, B. G., and Shanklin, J. D. (1985). Large losses of total ozone in Antarctica reveal seasonal ClOx/NOx interaction. *Nature*, *315*(6016), 207–210. https://doi.org/10.1038/315207a0

Frederick, J. E., Cebula, R. P., and Heath, D. F. (1986). Instrument characterization for the detection of long-term changes in stratospheric ozone: an analysis of the SBUY/2 radiometer. *J. Atmos. Oceanic Technol.*, *3*(3), 472–480. https://doi.org/10.1175/1520-0426(1986)003<0472:ICFTDO>2.0.CO;2

Fu, C., Li, W., and Zhou, X. (1997). *Simulation of the Formation of Ozone Low over Tibetan Plateau in Summer* (pp. 274-285). Beijing: Meteorological Press.

Fuhrer, J., and Booker, F. (2003). Ecological issues related to ozone: agricultural issues. *Environ. Int.*, 29(2-3), 141–154. https://doi.org/10.1016/S0160-4120(02)00157-5

Guo, D., Wang, P. X., Zhou, X. J., Liu, Y., and Li, W. L. (2012). Dynamic effects of the South Asian high on the ozone valley over the Tibetan Plateau. *Acta Meteor. Sin.*, 26(2), 216–228. https://doi.org/10.1007/s13351-012-0207-2

Guo, D., Su, Y. C., Shi, C. H., Xu, J. J., and Powell, Jr. A. M. (2015). Double core of ozone valley over the Tibetan Plateau and its possible Mechanisms. *J. Atmos. Solar-Terr. Phys.*, 130–131. https://doi.org/10.1016/j.jastp.2015.05.018

Guo, D., Su, Y. C., Zhou, X. J., Xu, J. J., Shi, C. H., Liu, Y., Li, W. L., and Li, Z. K. (2017a). Evaluation of the trend uncertainty in summer ozone valley over the Tibetan Plateau in three reanalysis datasets. *J. Meteor. Res.*, 31(2), 431–437. https://doi.org/10.1007/s13351-017-6058-x

Guo, D., Xu, J. J., Su, Y. C., Shi, C. H., Liu, Y., and Li, W. L. (2017b). Comparison of vertical structure and formation mechanism of summer ozone valley over the Tibetan Plateau and North America. *Trans. Atmos. Sci.* (in Chinese), 40(3), 412–417. https://doi.org/10.13878/j.cnki.dqkxxb.20160315001

Heath, D. F., Krueger, A. J., Roeder, H. R., and Henderson, B. D. (1975). The solar backscatter ultraviolet and total ozone mapping spectrometer (SBUV/TOMS) for NIMBUS G. *Opt. Eng.*, 14(4), 144323. https://doi.org/10.1117/12.7971839

Hilsenrath, E., Cebula, R. P., DeLand, M. T., Laamann, K., Taylor, S., Wellemeyer, C., and Bhartia, P. K. (1995). Calibration of the NOAA 11 solar backscatter ultraviolet (SBUV/2) ozone data set from 1989 to 1993 using in-flight calibration data and SSBUV. *J. Geophys. Res.: Atmos.*, 100(D1), 1351–1366. https://doi.org/10.1029/94JD02611

Levelt, P. F., Van den Oord, G. H. J., Dobber, M. R., Mälkki, A., Visser, H., De Vries, J., Stammes, P., Lundell, J. O. V., and Saari, H. (2006). The ozone monitoring instrument. *IEEE Trans. Geosci. Remote Sens.*, 44(5), 1093–1101. https://doi.org/10.1109/TGRS.2006.872333

Li, Z. K., Qin, H., Guo, D., Zhou, S. W., Huang, Y., Su, Y. C., Wang, L. W., and Sun, Y. (2017). Impact of ozone valley over the Tibetan Plateau on the South Asian high in CAM5. *Adv. Meteor.*, 2017, 9383495. https://doi.org/10.1155/2017/9383495

Liu, Y., Li, W. L., Zhou, X. J., and He, J. H. (2003). Mechanism of formation of the ozone valley over the Tibetan Plateau in summer-transport and chemical process of ozone. *Adv. Atmos. Sci.*, 20(1), 103–109. https://doi.org/10.1007/BF03342054

Liu, Y., Wang, Y., Liu, X., Cai, Z. N., and Chance, K. (2009). Tibetan middle tropospheric ozone minimum in June discovered from GOME observations. *Geophys. Res. Lett.*, 36(5), L05814. https://doi.org/10.1029/2008GL037056

Liu, Y., Li, W. L., and Zhou, X. J. (2010). A possible effect of heterogeneous reactions on the formation of the ozone valley over the Tibetan Plateau. *Acta Meteor. Sin.* (in Chinese), 68(6), 836–846. https://doi.org/10.11676/qxxb2010.079

McPeters, R. D., and Labow, G. J. (1996). An assessment of the accuracy of 14.5 years of Nimbus 7 TOMS version 7 ozone data by comparison with the Dobson network. *Geophys. Res. Lett.*, 23(25), 3695–3698. https://doi.org/10.1029/96GL03539

McPeters, R. D., Bhartia, P. K., Krueger, A. J., Herman, J. R., Wellemeyer, C. G., Seftor, C. J., Jaross, G., Torres, O., Moy, L., … Cebula, R. P. (1998). Earth probe total ozone mapping spectrometer (TOMS): data products user's guide. Maryland: NASA.

Molina, M. J., and Rowland, F. S. (1974). Stratospheric sink for chlorofluoromethanes: Chlorine atom- catalysed destruction of ozone. *Nature*, 249(5460), 820–812. https://doi.org/10.1038/249810a0

Moore, G. W. K., and Semple, J. L. (2005). A Tibetan Taylor Cap and a halo of stratospheric ozone over the Himalaya. *Geophys. Res. Lett.*, 32(21), L21810. https://doi.org/10.1029/2005GL024186

Nazaryan, H., McCormick, M. P., and Russell Ⅲ, J. M. (2005). New studies of SAGE Ⅱ and HALOE ozone profile and long-term change comparisons. *J. Geophys. Res.: Atmos.*, 110(D9), D09305. https://doi.org/10.1029/2004JD005425

Newman, P. A., Gleason, J. G., McPeters, R. D., and Stolarski, R. S. (1997). Anomalously low ozone over the Arctic. *Geophys. Res. Lett.*, 24(22), 2689–2692. https://doi.org/10.1029/97GL52831

Qin, H., Guo, D., Shi, C. H., Li, Z. K., Zhou, S. W., Huang, Y., Su, Y. C., and Wang, L. W. (2018). The interaction between variations of South Asia high and ozone in the adjacent regions. *Chin. J. Atmos. Sci.* (in Chinese), 42(2), 421–434. https://doi.org/10.3878/j.issn.1006-9895.1710.17159

Russell Ⅲ, J. M., Gordley, L. L., Park, J. H., Drayson, S. R., Hesketh, W. D., Cicerone, R. J., Tuck, A. F., Frederick, J. E., Harries, J. E., and Crutzen, P. J. (1993). The halogen occultation experiment. *J. Geophys. Res.: Atmos.*, 98(D6), 10777–10797. https://doi.org/10.1029/93JD00799

Russell Ⅲ, J. M., Gordley, L. L., Deaver, L. E., Thompson, R. E., and Park, J. H. (1994). An overview of the halogen occultation experiment (HALOE) and preliminary results. *Adv. Space Res.*, 14(9), 13–20. https://doi.org/10.1016/0273-1177(94)90110-4

Shi, C. H., Zhang, C. X., and Guo, D. (2017). Comparison of electrochemical concentration cell ozonesonde and microwave limb sounder satellite remote sensing ozone profiles for the center of the South Asian high. *Remote Sens.*, 9(10), 1012. https://doi.org/10.3390/rs9101012

Tian, W. S., Chipperfield, M., and Huang, Q. (2008). Effects of the Tibetan Plateau on total column ozone distribution. *Tellus B*, 60(4), 622–635. https://doi.org/10.1111/j.1600-0889.2008.00338.x

Tobo, Y., Iwasaka, Y., Zhang, D. Z., Shi, G. Y., Kim, Y. S., Tamura, K., and Ohashi, T. (2008). Summertime "ozone valley" over the Tibetan Plateau derived from ozonesondes and EP/TOMS data. *Geophys. Res. Lett.*, 35(16), L16801. https://doi.org/10.1029/2008GL034341

Van der Leun, J. C., Tang, X., and Tevini, M. (1995). Environmental effects of ozone depletion: 1994 assessment. *Ambio*, 24(3), 138–142.

Wang, W. G., Fan, W. X., Wu, J., Xie, Y. Q., Yuan, M., Chen, X. M., Yang, Q., and Wang, H. Y. (2006). A study of spatial-temporal evolvement of the global cross-tropopause ozone mass flux. *Chin. J. Geophys.*, 49(6), 1451–1466. https://doi.org/10.1002/cjg2.972

Waters, J. W., Read, W. G., Froidevaux, L., Jarnot, R. F., Cofield, R. E., Flower, D. A., Lau, G. K., Picketta, H. M., Santee, M. L., … Filipiak, M. J. (1999). The UARS and EOS microwave limb sounder (MLS) experiments. *J. Atmos. Sci.*, 56(2), 194–218. https://doi.org/10.1175/1520-0469(1999)056<0194:TUAEML>2.0.CO;2

Waters, J. W., Froidevaux, L., Jarnot, R. F., Read, W. G., Pickett, H. M., Harwood, R. S., Cofield, R. E., Filipiak, M. J., Flower, D. A., … Wu, D.L. (2004). *An overview of the EOS MLS experiment, Tech*. Rep.D-15745 Version 2.0, Jet Propul. Lab., Pasadena, Calif.

Waters, J. W., Froidevaux, L., Harwood, R. S., Jarnot, R. F., Pickett, H. M., Read, W. G., Siegel, P. H., Cofield, R. E., Filipiak, M. J., … Dodge, R. (2006). The earth observing system microwave limb sounder (EOS MLS) on the Aura satellite. *IEEE Trans. Geosci. Remote Sens.*, 44(5), 1075–1092. https://doi.org/10.1109/TGRS.2006.873771

Xie, F., Li, J. P., Tian, W. S., Fu, Q., Jin, F. F., Hu, Y. Y., Zhang, J. K., Wang, W. K., Sun, C., … Ding, R. Q. (2016). A connection from Arctic stratospheric ozone to El Niño-Southern oscillation. *Environ. Res. Lett.*, 11(12), 124026. https://doi.org/10.1088/1748-9326/11/12/124026

Yan, R. C., Bian, J. C., and Fan, Q. J. (2011). The impact of the South Asia high bimodality on the chemical composition of the upper troposphere and lower stratosphere. *Atmos. Oceanic Sci. Lett.*, 4(4), 229–234. https://doi.org/10.1080/16742834.2011.11446934

Yan, X. L., Zheng, X. D., Zhou, X. J., Vömel, H., Song, J. Y., Li, W., Ma, Y. H., and Zhang, Y. (2015). Validation of Aura Microwave Limb Sounder water vapor and ozone profiles over the Tibetan Plateau and its adjacent region during boreal summer. *Sci. China Earth Sci.*, 58(4), 589–603. https://doi.org/10.1007/s11430-014-5014-1

Ye, Z. J., and Xu, Y. F. (2003). Climate characteristics of ozone over Tibetan Plateau. *J. Geophys. Res.*, 108(D20), 4654. https://doi.org/10.1029/2002JD003139

Zhang, J. K., Tian, W. S., Xie, F., Tian, H. Y., Luo, J. L., Zhang, J., and Dhomse, S. (2014). Climate warming and decreasing total column ozone over the Tibetan Plateau during winter and spring. *Tellus B*, 66(1), 23415.

https://doi.org/10.3402/tellusb.v66.23415

Zhang, J. K., Tian, W. S., Xie, F., Chipperfield, M. P., Feng, W. H., Son, S. W., Abraham, N. L., Archibald, A. T., Bekki, S., … Zeng, G. (2018). Stratospheric ozone loss over the Eurasian continent induced by the polar vortex shift. *Nat. Commun., 9*(1), 206. https://doi.org/10.1038/s41467-017-02565-2

Zhou, S. W., and Zhang, R. H. (2005). Decadal variations of temperature and geopotential height over the Tibetan Plateau and their relations with Tibet

ozone depletion. *Geophys. Res. Lett., 32*(18), L18705. https://doi.org/10.1029/2005gl023496

Zhou, X. J., and Luo, C. (1994). Ozone valley over Tibetan Plateau. *Acta Meteor. Sin., 8*(4), 505–506.

Zou, H. (1996). Seasonal variation and trends of TOMS ozone over Tibet. *Geophys. Res. Lett., 23*(9), 1029–1032. https://doi.org/10.1029/96GL00767